Velocity modeling of supercritical pore fluids through porous media under reservoir conditions with applications for petroleum secondary migration and carbon sequestration plumes

Lauri A. Burke[1]

Abstract

Computational methods to characterize secondary migration in porous media traditionally rely on fluid transport equations with assumptions of time invariance, such as flow-path modeling of buoyancy vectors, statistical percolation algorithms, capillary pressure curves, or a form of Darcy's law, which presumes instantaneous fluid transport. However, in petroleum systems modeling, the timeframe of secondary migration from source to reservoir is important to quantify in relation to other geologic factors, such as the timing of petroleum generation, fault movement, and seal formation. In addition, quantifying migration velocities enables an estimation of the distance a plume of geologically sequestered carbon dioxide travels over time, as well as the identification of low-permeability strata appropriate for long-term containment. This study introduces a method to quantify transport velocities of supercritical fluids in low-permeability lithologies for a broad range of rock and fluid properties likely encountered in the sedimentary sequence. A time-dependent form of Darcy's law for pressure-driven viscous flow through homogeneous isotropic porous media was used to model flow velocities within a carrier bed. Thermodynamic equations of state were used to determine thermophysical properties of supercritical pore fluids under reservoir pressures ranging from 0 MPa to 200 MPa (0–29,000 psi) to constrain the momentum equations. Three case studies were examined that (1) estimated fluid flow velocities of methane within the low-permeability Upper Jurassic Haynesville Formation, (2) defined permeability-based flow units to evaluate saline formations for long-term geologic carbon sequestration, and (3) calculated the migration distance of carbon dioxide plumes at the Decatur, Illinois injection and sequestration project.

Introduction

Secondary migration of pore fluids through permeable carrier beds or along higher permeability fault and fracture systems is traditionally modeled using time-invariant transport equations, which assume instantaneous fluid flow. This time step is approached differently for modeling fluid transport processes in petrophysics and petroleum engineering occurring at production timeframes compared to secondary migration modeling for basin-scale analysis of petroleum systems over geologic timeframes (Figure 1). As an example of this differential treatment of time steps among disciplines, governing equations for natural gas transport in shale reservoirs are described by four scales of distance and time. These include molecular-collision fluid dynamics within the kerogen, microscale flow within the low-permeability matrix, grain-scale flow within the microfracture network, and mesoscale flow in the formation (Javadpour et al., 2007; Wang and Reed, 2009; Ozkan et al., 2010; Wei et al., 2018).

Carruthers (2003) determines that several input variables required for fluid transport modeling at reservoir scales and production time horizons are irrelevant for flow modeling of secondary migration at basin scales. The appropriate fluid transport equations for secondary migration in basin-scale modeling are described by buoyancy forces, capillary pressure, statistically defined invasion percolation, and a time-invariant form of Darcy's law (Hunt, 1996; Hantschel and Kauerauf, 2009). A harmonic average of buoyancy and capillary forces is appropriate to consider for secondary migration occurring vertically across stratigraphic layers (Schowalter, 1979); however, velocity is time invariant and assumed to be instantaneous.

In this study, a time-dependent form of Darcy's law was used to model fluid flow velocity within a

---

[1]U.S. Geological Survey, Denver, Colorado, USA. E-mail: lburke@usgs.gov (corresponding author).

low-permeability carrier bed. Fluid behaviors at reservoir conditions were determined from equations of state. The timeframe of secondary migration from source to reservoir is important in petroleum systems modeling to determine with respect to petroleum generation, fault movement, and seal formation. In addition, quantifying pore fluid migration velocities has direct applications in evaluating formations for geologic sequestration and long-term storage of carbon dioxide greenhouse gas.

In contrast to traditional methods for modeling secondary migration, which assume time invariance of fluid transport, this study's numerical modeling objectives were fourfold: (1) quantify secondary migration velocities for supercritical fluids through porous media under reservoir pressure and temperature conditions, (2) use these velocities to calculate secondary migration distances within a given carrier bed, (3) use secondary migration velocities to calculate the transit time of these fluids, and (4) evaluate long-term storage and containment of sequestered fluids based on permeability-based flow units.

Numerical models for methane and carbon dioxide were developed to study secondary migration velocity over a broad range of reservoir pressures (0–200 MPa [0–29,000 psi]). A reservoir temperature of 177°C ± 6°C (350°F ± 20°F) was chosen for case study 1 involving methane , and a reservoir temperature of 93°C ± 6°C (200°F ± 20°F) was chosen for case studies 2 and 3 involving CO_2 migration, based on values available in research studies (Burke, 2011; Wang et al., 2013). The spectrum of porosities (ϕ = 0%–95%) and 15 permeability magnitudes (κ = 10 D–0.1 nD) encompass a substantial range of possible rock property combinations encountered in the sedimentary sequence. Three case studies demonstrate the application and interpretation of these modeling results specifically for (1) quantifying migration velocities of methane within a low-permeability carrier bed exhibiting representative rock properties of the Upper Jurassic Haynesville Formation

Figure 1. Venn diagram of fluid transport models for Newtonian fluids (after Burke, 2021).

of the U.S. Gulf Coast petroleum system, (2) defining permeability-based flow units of saline formations that are potentially targeted for geologic carbon sequestration, and (3) estimating long-term migration distances and containment timescales of geologically sequestered carbon dioxide plumes. Given the broad range of properties represented in these models, velocity results are applicable for an array of methane-bearing petroleum systems and geologic sequestration targets.

Methodology

The fluid transport methodology introduced in this study is summarized in Figure 2. In continuum fluid dynamics, the Navier-Stokes momentum equations are the constitutive relations for describing the flow of a Newtonian fluid. Fluids typically encountered in the sedimentary sequence adhere to Newtonian fluid behavior in which viscosity remains constant with the application of shear stress; a rare exception is emulsified bitumen (Bazyleva et al., 2010). Darcy's law is a general solution of the Navier-Stokes equations that are appropriate for describing the laminar flow of a viscous Newtonian fluid through a homogeneous isotropic media under a pressure differential. A time-dependent form of Darcy's law was used to quantify flow vectors in this study.

Derivation of Darcy's law as a general solution of the Navier-Stokes equations (Whitaker, 1985) to mathematically verify Darcy's empirical findings (Darcy, 1856) describes pressure-driven fluid flow through porous media as a proportional relation among the matrix permeability κ, fluid viscosity η, and pressure gradient over a distance $\Delta P/L$. The Darcy flow rate Q is defined as

$$Q = \frac{\kappa A}{\eta} \frac{\Delta P}{L}, \tag{1}$$

for Darcy flow through pore throats with cross-sectional area A. Darcy flux is obtained when this expression is solved in terms of velocity $\mathbf{v}$. Darcy flux divided by porosity ϕ yields the interstitial pore velocity:

$$\mathbf{v} = \frac{\kappa \Delta P}{\eta \phi L}, \tag{2}$$

as a function of reservoir fluid and rock properties. When solving in terms of time τ_D, the interstitial pore velocity for pressure-driven laminar fluid transport through porous media can be expressed as

$$\tau_D = \frac{\eta \phi L^2}{\kappa \Delta P}, \tag{3}$$

where ϕ represents matrix porosity.

Constitutive laws used to describe thermophysical properties of supercritical fluids under reservoir pressure and temperature conditions are discussed in the following section. Matrix porosity and permeability are used to condition the momentum equations. Model
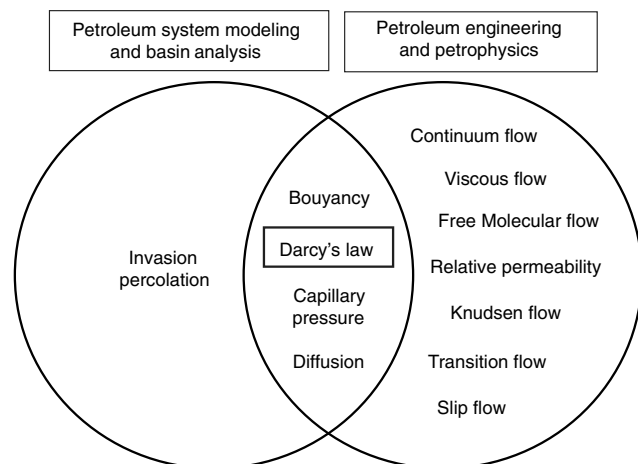
outputs quantify migration timescales. By using a 1.0 km distance, interstitial pore fluid velocities can be obtained.

Thermophysical properties

Constitutive laws describing thermophysical properties as a function of pressure and temperature are used to condition the Navier Stokes and the continuity momentum equations (Figure 2). Thermophysical properties for fluid density, fluid viscosity, fluid compressional-wave (P-wave) velocity, and fluid compressibility shown for methane (Figure 3a–3d) and for CO_2 (Figure 3e–3h) are obtained using the reference fluid thermodynamic and transport properties database (NIST, 2019). Equations of state for supercritical methane (Younglove and Ely, 1987; Setzmann and Wagner, 1991; Richter and McLinden, 2014) are used to obtain thermophysical properties based on the reference fluid thermodynamic and transport properties database (NIST, 2019) for pressures ranging from 0MPa to 200 MPa (0–29,000 psi) at isothermal conditions of 350°F (177°C). Similarly, equations of state for supercritical CO_2 (Span and Wagner, 1996; Lemmon et al., 2011) are used to obtain CO_2 thermophysical properties using the thermodynamic database (NIST, 2019) for pressures ranging from 0 MPa to 200 MPa (0–29,000 psi) at isothermal conditions of 93°C (200°F). This broad pressure range is inclusive of pressure conditions likely encountered in the sedimentary sequence, considering that the deepest producing wells reach 9144 m (30,000 ft; Dyman and Cook, 1998) and the standard definition of a 1.0 psi/ft lithostatic pressure gradient at depths of 9144 m (30,000 ft) yields 206.8 MPa (30,000 psi/ft).

Thermophysical properties for fluid compressibility of supercritical methane (Figure 3d) and CO_2 (Figure 3h) as a function of pressure are calculated using the Newton-Laplace equation from the methodology by Burke (2011). The Newton-Laplace equation relates the square of fluid P-wave velocity V_P as a function of fluid density ρ_f and elastic moduli K and μ as

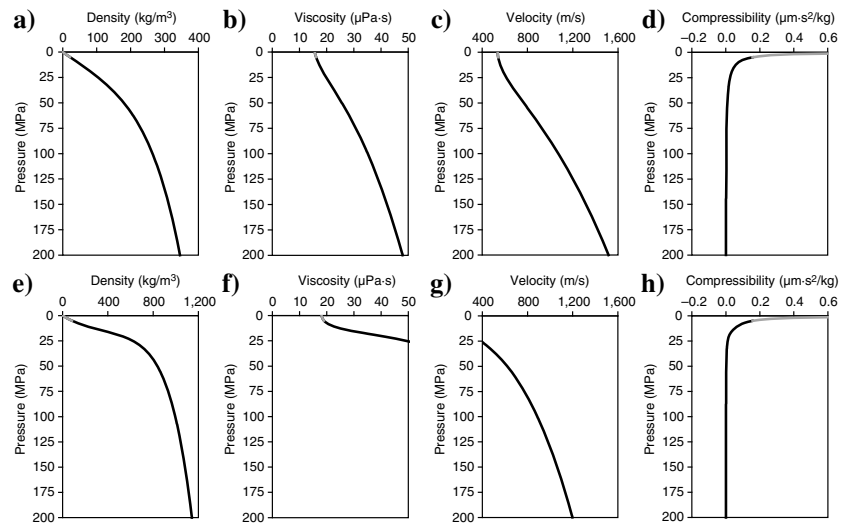$$V_P^2 = [(K + 4/3\mu)/\rho]. \tag{4}$$

Figure 3. (a-h) Thermophysical properties of methane and carbon dioxide.
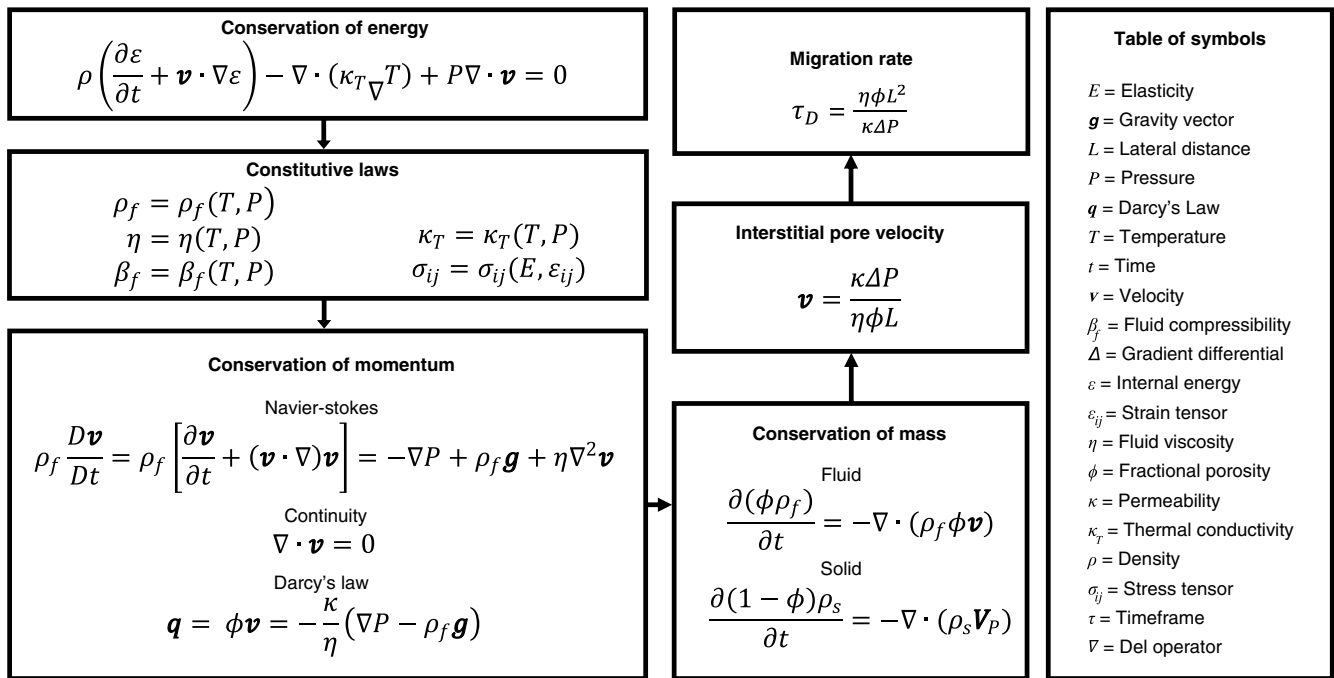

Figure 2. Workflow diagram of the fluid flow transport methodology developed in this study.

Newtonian fluids generally do not propagate shear stresses; thus, shear modulus $\mu = 0$. Fluid compressibility is obtained from the inverse of fluid bulk modulus K.

Fluid densities for supercritical methane and CO_2 (Figure 3a and 3e) rapidly increase with pressure. With increasing pressure, the viscosity of methane exhibits almost linear behavior (Figure 3b), whereas CO_2 viscosity approaches asymptotic behavior approximately 25 MPa (Figure 3f). The fluid P-wave velocity of supercritical methane increases linearly as a function of pressure (Figure 3c), whereas the velocity of CO_2 rapidly increases with pressure conditions (Figure 3g). Fluid compressibility for both fluids is strongly influenced by increasing pressure up to approximately 25 MPa, at which point compressibility attains a minimum value (Figure 3d and 3h).

Thermophysical properties of methane and CO_2 vary as a function of volume, pressure, and temperature. Calculations of thermophysical properties from NIST (2019) require an assumption to be made for either isochoric, isopressure, or isothermal conditions. Pore pressure increases in the rocks from, for example, buoyancy or volumetric expansion as fluid propagates, are taken into account by the pressure component in the Darcy equation. Pressure conditions are expected to have a much greater influence on the thermophysical properties of interest in this migration model (i.e., fluid density, viscosity P-wave velocity, and compressibility) than the small temperature differentials associated with geothermal gradients during migration within a carrier bed. Thus, a wide range of pressures are incorporated into the models by making the reasonable assumption of isothermal conditions. The "Sensitivity analysis" section discusses the implications of this assumption on the thermophysical properties and resultant migration velocities.

Modeling results

Secondary migration velocities are calculated for a substantial range of rock and fluid properties and are shown for 15 orders of magnitude in permeability for a wide range of porosities from 0% to 95% (Figure 4). Figure 4a shows that carrier beds with permeabilities in the Darcy (D) range correspond to migration velocities from 3×10^{-4} to 3×10^{-1} m/s. Carrier beds with millidarcy (mD) permeabilities (Figure 4b) correspond to migration velocities from 3×10^{-7} to 3×10^{-4} m/s. Migration velocities within carrier beds measured in microdarcy (μD) permeabilities (Figure 4c) fall within the 3×10^{-10} to 3×10^{-7} m/s velocity range. Figure 4d shows that rock properties in the nanodarcys (nD) range correspond to migration velocities from 3×10^{-13} to 3×10^{-10} m/s. For completeness, permeabilities in the picodarcy range (not shown) represent the extreme lower bound in this model and correspond to migration velocities slower than 3×10^{-13} m/s, which is equivalent to a timeframe of billions of years, exceeding the tectonic cycle of most sedimentary basins. Depending on the formation permeability of interest, Figure 4 can be used to research and estimate the migration velocity by any given porosity value.

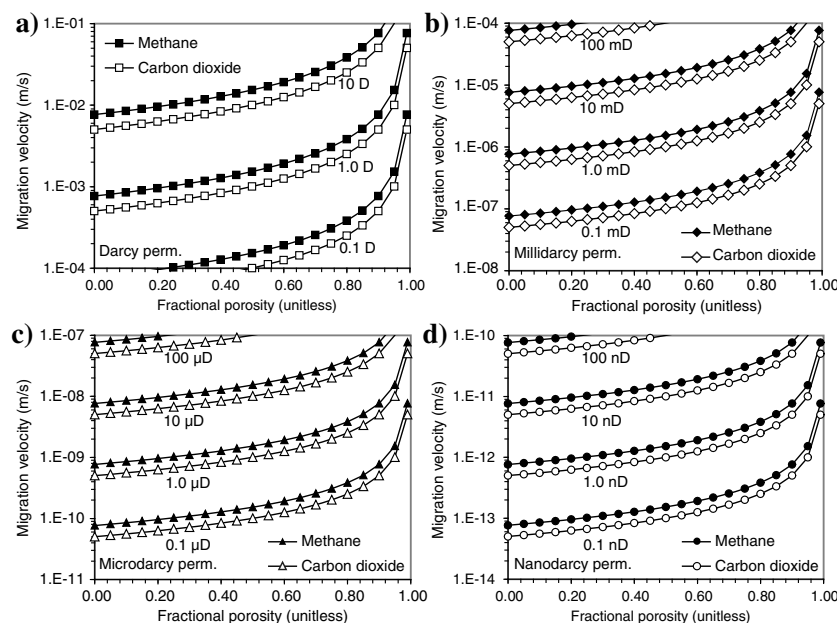By normalizing migration through a 1.0 km carrier bed, conversion from

Figure 4. (a-d) Migration velocities of methane and carbon dioxide under reservoir conditions for 15 orders of magnitude.

Table 1. Sample conversion from velocity to timescale for several orders of magnitude quantified in this model.

Velocity (m/s)	Velocity (km/yr)	Timescale (yr)	Timescale as a fraction of year	Analog
1.00E−01	3.15E+03	3.17E−04	1.16E−01	Months
1.00E−04	3.15E+00	3.17E−01	1.16E+02	Centuries
1.00E−07	3.15E−03	3.17E+02	1.16E+05	100,000 years
1.00E−10	3.15E−06	3.17E+05	1.16E+08	100 Ma
1.00E−13	3.15E−09	3.17E+08	1.16E+11	Billions of years

velocity to timescale in years (yrs) can be computed. Table 1 summarizes these results, which also are available in the associated data release (Burke, 2022). Case studies in the next three sections illustrate the application and interpretation of this quantitative migration modeling.

Sensitivity analysis

The influences of porosity, permeability, pressure, temperature, and saturation on migration velocity are investigated. According to this sensitivity analysis, the principle factors affecting migration velocities are the porosity and permeability of the carrier beds. Higher porosities and permeabilities correspond to increases in migration velocities and reductions in timescales. Pressure influences thermophysical properties of methane and CO_2; thus, a wide range of pressures from 0 MPa to 200 MPa (0–29,000 psi) are studied. Pressure also is accounted for in Darcy's law. Higher pressures correspond to faster migration velocities and reduced timescales. However, changes in reservoir temperature along a carrier bed are expected to be scalar values and not exponential. Scalar changes in temperature would minimally affect density, viscosity, and P-wave velocity of the fluid, which would result in a negligible influence on migration velocities and timescales. Fluid compressibility asymptotically approaches a minimum value and remains invariant to temperature changes at these reservoir pressures. Investigation of various methane-water and CO_2-water fluid saturations are investigated at 25% increments, for example, 25% methane and 75% water. Results indicate that saturation influences fluid density, viscosity, and velocity in a linear fashion that is well below the resolution of this order-of-magnitude modeling technique.

Case study 1

The Haynesville Formation of the onshore U.S. Gulf Coast is an important domestic resource for petroleum. U.S. Geological Survey (USGS) assessments of undiscovered, technically recoverable resources estimate the Haynesville Formation contains means of 1.1 billion barrels of oil, a mean of 195.8 trillion cubic feet of natural gas, and a mean of 0.9 billion barrels of natural gas liquids

(Paxton et al., 2018). Although the Haynesville is widely considered to be a self-sourced natural gas reservoir (Wang and Hammes, 2010; Hammes et al., 2011), the Haynesville and underlying Smackover source rocks are not thermally mature enough to generate the large volumes of dry gas produced along the southeastern margin of the Sabine uplift area in Louisiana (Paxton et al., 2021). However, Haynesville and Smackover Formation source rocks are generating dry gas in the adjacent North Louisiana Salt Basin (Torsch, 2012). Quantifying secondary migration velocities may reveal if the low-permeability Haynesville could represent a feasible migration pathway over a reasonable geologic timeframe.

Secondary migration velocities are modeled using average reservoir temperature (T = 177°C or 350°F) and representative rock properties (ϕ = 9%; κ = 400 nD) of the Haynesville Formation (Table 2) after Wang et al. (2013). Accordingly, a reservoir temperature of 177°C (350°F) is used to condition pore fluid thermophysical properties over a broad range of reservoir pressures from 0 MPa to 200 MPa (0 to 29,000 psi). Modeling results (Figure 4d) indicate that interstitial pore fluid velocity is 3×10^{-10} m/s, which corresponds to 1×10^5 years (100,000 years) for secondary migration to transit 1.0 km of these low-permeability carrier beds. The distance from thermally mature Jurassic source rocks in the middle of North Louisiana Salt Basin to the center of the productive trend of the Haynesville Formation in the Sabine uplift area is approximately 155 km (96 mi). Given this velocity and distance, 15.5 million years (Ma) are required for secondary migration of dry gas in this example pathway, which is beyond the production timeframe of transporting fluids from the reservoir into the wellbore but well within the geologic timeframe to charge a reservoir. Thus, the potential exists for additional hydrocarbon charges to have originated in an adjacent basin due to fluid flow based on Darcy's law.

Case study 2

Geologic sequestration and long-term subsurface storage of supercritical CO_2 represent a solution for decreasing atmospheric emissions of this anthropogenic greenhouse gas (Benson and Cole, 2008). Identification of appropriate saline formations for CO_2

Table 2. Reservoir conditions and representative formation properties of the upper Jurassic Haynesville Formation (after Wang et al., 2013).

Reservoir property	Range (English)	Range (metric)	Average (English)	Average (metric)
Depth	10,000–18,000 ft	3048–5486 m	14,000 ft	4267 m
Reservoir pressure	8000–17,000 psi	55.2–117.2 MPa	12,500 psi	86.2 MPa
Pressure gradient	0.70–0.95 psi/ft	15.8–21.5 kPa/m	0.83 psi/ft	18.8 kPa/m
Reservoir temperature	260°F–430°F	127°C–221°C	345°F	174°C
Porosity	3%–14%	3%–14%	9%	9%
Permeability	400 nD	3.948×10^{-19} m^2	400 nD	3.948×10^{-19} m^2

containment can be determined, in part, from the velocity and timeframe that fluids migrate through them. Supercritical CO_2 migration velocities are modeled (Burke, 2011) for a broad range of porosities and permeabilities likely encountered in the sedimentary sequence (Table 3). Based on the geothermal gradient and target formation depth, an average reservoir temperature of 93°C (200°F) is used (Burke, 2011) to constrain pore fluid thermophysical properties over reservoir pressures ranging from 0 MPa to 200 MPa (0–29,000 psi).

Modeling results (Figure 4) are shown as a function of porosity. For a storage formation with 1.0 D permeability (Figure 4a) and 10% porosity, results indicate that interstitial pore fluid velocity is 3×10^{-3} m/s, which corresponds to days to weeks for migration of these pore fluids to transit 1.0 km of the storage formation. Similarly, migration velocity through porous media with 1.0 mD permeability (Figure 4b) and 10% porosity is 3×10^{-6} m/s, which corresponds to 94.6 m/yr. This implies decades of containment for millidarcy permeability rocks exhibiting porosities approximately 10%. Migration velocity through 1.0 μD permeability (Figure 4c) strata at 10% porosity is 3×10^{-9} m/s, which corresponds to 9.46×10^{-2} m/yr for containment spanning centuries to millennia. Migration velocity through 1.0 nD permeability strata (Figure 4d) with 10% porosity is 3×10^{-12} m/s, which corresponds to 9.46×10^{-5} m/yr, representing several million years of containment; however, injections pressures required to sequester fluid in this strata are unfeasible with present engineering technology. Migration velocities in media with picodarcy permeabilities (3×10^{-15} m/s; not shown) could theoretically harbor fluids for billions of years, which exceed the tectonic cycle of most sedimentary basins. This migration model was developed to quantify supercritical CO_2 flow timescales (Burke, 2011) as a way to divide the subsurface into permeability-based flow units in support of the USGS methodology to assess the storage capacity of sequestered carbon dioxide into saline formations (Burruss et al., 2009; Brennan et al., 2010).

Case study 3

The Illinois Basin-Decatur Project is the world's first large-scale carbon capture and storage demonstration project from a biofuel source in which 1.1 million tons of CO_2 are sequestered over a three-year period from 2011 to 2014 at an injection rate of 1000 tons per day (Gollakotaa and McDonald, 2014; Bauer et al., 2016). At this site, the Mesoproterozoic (1467 ± 25 Ma) basement is fractured rhyolite with a clay-rich matrix, and it is unconformably overlain by thin (approximately 33 m or approximately 100 ft) low permeability fine- to medium-grained sandstones (Leetaru and Freiburg, 2014), which are informally known as the Cambrian pre-Mount Simon interval (Freiburg et al., 2014). The 2130 m (7000 ft) deep target formation is the upper Cambrian Mount Simon sandstone, which is a 460 m (1500 ft) thick sand-rich fluvial system containing braid plain, flood plain, alluvium, and playa deposits (Leetaru and Freiburg, 2014). The regionally extensive middle to upper Cambrian Eau Claire Formation, comprised of low-permeability siltstones and mudstones, forms the 100–150 m (330–500 ft) thick primary seal preventing buoyant CO_2 migration into the overlying strata; the upper Ordovician Maquoketa Shale Group at 820 m (2700 ft) and the Devonian New Albany Shale at 650 m (2100 ft) form the shallower secondary and tertiary seals (Leetaru and Freiburg, 2014), respectively.

Four textural facies are interpreted within the Mount Simon, including unbleached fine-grained and coarse-grained sandstone beds, as well as bleached fine-grained and coarse-grained sandstone beds (Ritzi et al., 2016). Although the specific cause of bleaching in the Mount Simon is unknown (Ghose, 2017), Ritzi et al. (2016) observe permeability reduction and porosity loss due to pore cementation and mechanical compaction in the bleached intervals, as compared with unbleached intervals. Average porosity and permeability for each of these textural lithofacies are given in Table 4 (Ghose, 2017); the representative Mount Simon rock properties for our velocity modeling are $\phi = 17\%$ and $\kappa = 45$ mD. Migration velocities are modeled through 1.0 km of isotropic porous media exhibiting these rock properties while using a reservoir temperature of 93°C (200°F) to condition the thermophysical properties of fluid density, fluid viscosity, fluid P-wave transit time, and fluid compressibility over reservoir pressures ranging from 0 MPa to 200 MPa (0–29,000 psi). The wellhead injection pressure

Table 3. Summary of select reservoir properties to study carbon dioxide geologic sequestration and storage (after Burke, 2011).

Reservoir property	Range (English)	Range (metric)	Average (English)	Average (metric)
Depth	3000–13,000 ft	900–4000 m	8000 ft	2440 m
Reservoir pressure	0–29,000 psi	0–200 MPa	3720 psi	25.5 MPa
Pressure gradient	0.433–0.600 psi/ft	9.49–13.57 kPa/m	0.465 psi/ft	10.52 kPa/m
Reservoir temperature	150°F–250°F	66°C–120°C	200°F	93°C
Porosity	0%–95%	0%–95%	10%	10%
Permeability	1.0 D–1.0 pD	9.87×10^{-13}–9.87×10^{-25} m^2	100 mD	9.87×10^{-17} m^2

is approximately 9.3 MPa (1350 psi) ([Finley et al., 2013](#)). A hydrostatic pressure of 9.8 kPa/m (0.433 psi/ft) in the reservoir at 2,130 m (7,000 ft) in depth yields a reservoir pressure of 20.9 MPa (3,031 psi) and a pressure differential away from the turbulent flow of the injection plume is 11.6 MPa (1,681 psi). This results in a migration velocity of 6.06×10^{-5} m/s, which equates to 1910 m/yr or a distance of 19 km (11.8 mi) in the 10 years after injection began; however, this upper bound estimate assumes no pressure decay. According to an analog carbon capture and storage project in Shenhua, China ([Zhu et al., 2015](#)), 20%–50% of this upper bound is more realistic and takes into account the geomechanical response of the formation after carbon sequestration concludes. Therefore, the CO_2 plume may have migrated 3.8 km (2.4 mi) and as far as 9.5 km (5.9 mi) away from the injection wellbore. USGS passive seismic monitoring of this site has shown no increase in the number or magnitude of microseismicity events either radially away from the wellbore or occurring at depths other than the injection zone ([Kavern et al., 2015](#);[Bauer et al., 2016](#)). Monitoring for potential leakage includes inspection of wellhead equipment, pressure monitoring of the CO_2 plume, neutron tracer logging, and groundwater quality monitoring during the injection phase and extending 50 years after injection ends; the most likely leakage pathway is expected to be through aging wellhead and pipeline equipment and not a geologic pathway ([Gollakotaa and McDonald, 2014](#)).

Discussion

The model examines wellbore, reservoir, and basin scales of investigation; nanoscale molecular interactions at the fluid-mineral interface are not taken into account. Navier-Stokes momentum equations are used to describe the fluid dynamics of the system; chemical dissolution into other fluid phases or chemical reactions at the fluid-solid interface are beyond the scope of this study. The constitutive laws rely on fluid properties as a function of pressure and a representative temperature. Large changes in pressure may influence fluid properties; thus, a wide range of pressures is accounted for in the model. Linear changes in fluid temperature, as may be expected from fluid migration originating deeper in the basin, would have a negligible influence on fluid density, fluid compressibility, and fluid viscosity, resulting in a negligible influence on the resultant

migration velocities and timescales. The model assumes fluid transport through homogeneous media in which representative rock properties are used as inputs. This scenario does not specifically account for porosity heterogeneity or permeability variation within the carrier bed; variation in rock properties can be accounted for by taking the weighted average of the resultant velocities from a series of models each with relevant ϕ-κ combinations. Note that fault and fracture networks can be approximated by higher porosities and permeabilities. These models examined the migration velocities of methane and CO_2, which have molecular masses of 16.04 and 44.01 atomic mass units (amu), respectively. Heavier hydrocarbons are expected to decrease the resultant migration velocity. For example, ethane and propane (30.07 amu and 44.1 amu, respectively) presumably plot between methane and CO_2 shown in Figure [4](#) velocity plots.

Conclusion

This study introduces a quantitative methodology for calculating migration velocities of supercritical pore fluids through porous media under reservoir temperature and pressure conditions. Constitutive laws and equations of state are used to obtain the thermophysical fluid properties used to condition a time-dependent derivation of Darcy's law for calculating fluid transit through a wide range of porosity and permeability carrier beds likely encountered in the sedimentary sequence. Three case studies demonstrate the application of this migration velocity modeling. Fluid flow velocities of methane are modeled to determine that potential exists for additional hydrocarbon charge of the Haynesville Formation to have originated in and migrated from an adjacent basin. This migration model is further adapted for calculating velocities of supercritical CO_2 migration in porous media as a means to identify permeability-based containment formations appropriate for geologic sequestration and long-term storage of this greenhouse gas. The model also is used to estimate the 3.8 km (2.4 mi) distance that geologically sequestered CO_2 could be expected to migrate radially from the injection wellbore at the Illinois Basin-Decatur project, a large-scale carbon capture, and storage demonstration project. The model is applicable for a wide range of reservoir conditions (0–200 MPa or 0–29,000 psi) and rock properties (ϕ = 0%–95%; κ = 10

Table 4. Porosity and permeability by textual facies interpreted within the upper Cambrian Mount Simon sandstone (after [Ghose, 2017](#)).

Textural facies	Porosity (%)	Permeability (mD)	Permeability (m²)	Percent of the reservoir (%)
Unbleached finer grained	20	10	9.87×10^{-18}	8
Unbleached coarser grained	20	100	9.87×10^{-17}	32
Bleached finer grained	15	2.5	2.47×10^{-18}	12
Bleached coarser grained	15	25	2.47×10^{-17}	48

D–0.1 nD); the model can be adapted to accommodate other temperature conditions and geologic scenarios.

Data and materials availability

Data tables associated with this modeling include migration velocities and timescales for supercritical methane and carbon dioxide (Burke, 2022).

References

Bauer, R. A., M. Carney, and R. J. Finley, 2016, Overview of microseismic response to CO_2 injection into the Mt. Simon saline reservoir at the Illinois Basin-Decatur Project: International Journal of Greenhouse Gas Control, 54, 378–388, doi: 10.1016/j.ijggc.2015.12.015.

Bazyleva, A. B., A. Hasan, M. Fulem, M. Becerra, and J. M. Shaw, 2010, Bitumen and heavy oil rheological properties: Reconciliation with viscosity measurements: Journal of Chemical and Engineering Data, 55, 1389–1397, doi: 10.1021/je900562u.

Benson, S. M., and D. R. Cole, 2008, CO_2 sequestration in deep sedimentary formations: Elements, 4, 325–331, doi: 10.2113/gselements.4.5.325.

Brennan, S. T., R. C. Burruss, M. D. Merrill, P. A. Freeman, and L. F. Ruppert, 2010, A probabilistic assessment methodology for the evaluation of geologic carbon dioxide storage: U.S. Geological Survey Open-File Report 2010–1127, 31.

Burke, L. A., 2011, Carbon dioxide fluid-flow modeling and injectivity calculations: U.S. Geological Survey Scientific Investigations Report 2011–5083, 16.

Burke, L. A., 2021, Quantitative modeling of secondary migration: Understanding the origin of natural gas charge of the Haynesville Formation in the Sabine Uplift area of Louisiana and Texas: GCAGS Journal, 10, 16–24.

Burke, L. A., 2022, Data tables associated with velocity modeling of supercritical pore fluids through porous media at reservoir conditions with applications for petroleum secondary migration and carbon sequestration plumes: U.S. Geological Survey Data Release, doi: 10.5066/P9GT9TWK.

Burruss, R. C., S. T. Brennan, P. A. Freeman, M. D. Merrill, L. F. Ruppert, M. F. Becker, W. N. Herkelrath, Y. K. Kharaka, C. E. Neuzil, S. M. Swanson, T. A. Cook, T. R. Klett, P. H. Nelson, and C. J. Schenk, 2009, Development of a probabilistic assessment methodology for evaluation of carbon dioxide storage: U.S. Geological Survey Open-File Report 2009–1035, 81.

Carruthers, D. J., 2003, Modeling of secondary petroleum migration using invasion percolation techniques, in S. Duppenbecker and R. Marzi, eds., Multidimensional basin modeling: AAPG, Datapages Discovery Series 7, 21–37.

Darcy, H. P. C., 1856, Les fontaines publiques de la Ville de Dijon: Victor Dalmont.

Dyman, T. S., and T. A. Cook, 1998, Summary of deep oil and gas wells in the United States through 1998: U.S. Geological Survey, Digital Data Series 067, 7.

Finley, R. J., S. M. Failey, H. E. Leetaru, O. Senel, M. L. Coueslan, and M. Scott, 2013, Early operational experience at a one-million tonne CCS demonstration project, Decatur, Illinois, USA: Energy Procedia, 37, 6149–6155, doi: 10.1016/j.egypro.2013.06.544.

Freiburg, J. T., D. G. Morse, H. E. Leetaru, R. P. Hoss, and Q. Yan, 2014, A depositional and diagenetic characterization of the Mt. Simon sandstone at the Illinois Basin-Decatur Project carbon capture and storage site, Decatur, Illinois, USA: Illinois State Geological Survey, Circular 583, 70.

Ghose, R. C., 2017, Linking the variance of permeability and porosity to newly interpreted lithofacies at the site of the Illinois Basin-Decatur Project, Decatur, Illinois: M.S. thesis, Wright State University, 32.

Gollakotaa, S., and S. McDonald, 2014, Commercial-scale CCS project in Decatur, Illinois — Construction status and operational plans for demonstration: Energy Procedia, 63, 5986–5993, doi: 10.1016/j.egypro.2014.11.633.

Hammes, U., H. S. Hamlin, and T. E. Ewing, 2011, Geologic analysis of the Upper Jurassic Haynesville Shale in east Texas and west Louisiana: AAPG Bulletin, 95, 1643–1666, doi: 10.1306/02141110128.

Hantschel, T., and A. I. Kauerauf, 2009, Fundamentals of basin and petroleum systems modeling: Springer, 486.

Hunt, J. M., 1996, Petroleum geochemistry and geology, 2nd ed.: W. H. Freeman, 743.

Javadpour, F., D. Fisher, and M. Unsworth, 2007, Nanoscale gas flow in shale gas sediments: Journal of Canadian Petroleum Technology, 46, 10, doi: 10.2118/07-10-06.

Kavern, J. O., S. H. Hickman, A. F. McGarr, and W. L. Ellsworth, 2015, Surface monitoring of microseismicity at the Decatur, Illinois, CO_2 sequestration demonstration site: Seismological Research Letters, 86, 1096–1101, doi: 10.1785/0220150062.

Leetaru, H. E., and J. T. Freiburg, 2014, Litho-facies and reservoir characterization of the Mt Simon Sandstone at the Illinois Basin-Decatur Project: Greenhouse Gases: Science and Technology, 4, 580–595, doi: 10.1002/ghg.1453.

Lemmon, E. W., M. O. McLinden, and D. G. Friend, 2011, Thermophysical properties of fluid systems in NIST chemistry webbook, in P. J. Linstrom and W. G. Mallard, eds., NIST standard reference database number 69: National Institute of Standards and Technology.

NIST, 2019, National Institute of Standards and Technology reference fluid thermodynamic and transport properties database (REFPROP version 7): U.S. Department of Commerce.

Ozkan, E., R. S. Raghavan, and O. G. Apaydin, 2010, Modeling of fluid transfer from shale matrix to fracture network: Presented at the Annual Technical Conference and Exhibition, SPE.

Paxton, S. T., J. K. Pitman, L. A. Burke, and S. A. Kinney, 2021, Evidence for an Upper Jurassic Smackover source of natural gas in the overpressured Upper Jurassic Haynesville Formation, Sabine Uplift of Louisiana, USA: Presented at the Annual Convention and Exhibition, AAPG.

Paxton, S. T., J. K. Pitman, S. A. Kinney, N. J. Gianoutsos, O. N. Pearson, K. J. Whidden, R. F. Dubiel, C. J. Schenk, L. A. Burke, T. R. Klett, H. M. Leathers-Miller, T. J. Mercier, S. S. Haines, B. A. Varela, P. A. Le, T. M. Finn, S. B. Gaswirth, S. J. Hawkins, K. R. Marra, and M. E. Tennyson, 2018, U.S. Geological Survey input-data forms for the assessment of the Upper Jurassic Haynesville Formation, U.S. Gulf Coast, 2016: U.S. Geological Survey Open-File Report 2018–1130, 62.

Richter, M., and M. O. McLinden, 2014, Vapor-phase (p, ρ, T, x) behavior and virial coefficients for the (methane + propane) system: Journal of Chemical Engineering Data, **59**, 4151–4164, doi: 10.1021/je500792x.

Ritzi, R. W., J. T. Freiburg, and N. D. Webb, 2016, Understanding the (co)variance in petrophysical properties of CO_2 reservoirs comprising sedimentary architecture: International Journal of Greenhouse Gas Control, **51**, 423–434, doi: 10.1016/j.ijggc.2016.05.001.

Schowalter, T. T., 1979, Mechanics of secondary hydrocarbon migration and entrapment: AAPG Bulletin, **63**, 723–760, doi: 10.1306/2F9182CA-16CE-11D7-8645000102C1865D.

Setzmann, U., and W. Wagner, 1991, A new equation of state and tables of thermodynamic properties for methane covering the range from the melting line to 625 K at pressures up to 1000 MPa: Journal of Physical Chemistry Reference Data, **20**, 1061–1155, doi: 10.1063/1.555898.

Span, R., and W. Wagner, 1996, A new equation of state for carbon dioxide covering the fluid region from the triple-point temperature to 1100 K at pressures up to 800 MPa:

Journal of Physical and Chemical Reference Data, **25**, 1509–1596, doi: 10.1063/1.555991.

Torsch, W. C., 2012, Thermal and pore pressure history of the Haynesville Shale in north Louisiana: A numerical study of hydrocarbon generation, overpressure, and natural hydraulic fractures: M.S. thesis, Louisiana State University, Baton Rouge, Louisiana, 82.

Wang, F. P., and U. Hammes, 2010, Effects of petrophysical factors on Haynesville fluid flow and production: World Oil, **231**, D79–D82.

Wang, F. P., U. Hammes, and Q. Li, 2013, Overview of Haynesville shale properties and production, *in* U. Hammes and J. Gale, eds., Geology of the Haynesville gas shale in East Texas and West Louisiana, U.S.A.: AAPG Memoir, **105**, 155–177.

Wang, F. P., and R. M. Reed, 2009, Pore networks and fluid flow in gas shales: Presented at the Annual Technical Conference and Exhibition, SPE.

Wei, M., J. Lui, D. Elsworth, and E. Wang, 2018, Triple-porosity modelling for the simulation of multiscale flow mechanisms in shale reservoirs: Geofluids, **2018**, 1, doi: 10.1155/2018/6948726.

Whitaker, S., 1985, Flow in porous media I: A theoretical derivation of Darcy's law: Transport in Porous Media, **1**, 3–25, doi: 10.1007/BF01036523.

Younglove, B. A., and J. F. Ely, 1987, Thermophysical properties of fluids II: Methane, ethane, propane, isobutane, and normal butane: Journal of Physical and Chemical Reference Data, **16**, 577–798, doi: 10.1063/1.555785.

Zhu, Q., D. Zuo, S. Zhang, Y. Zhang, Y. Wang, and L. Wang, 2015, Simulation of geomechanical responses of reservoirs induced by CO_2 multilayer injection in the Shenhua CCS project, China: International Journal of Greenhouse Gas Control, **42**, 405–414, doi: 10.1016/j.ijggc.2015.08.017.

A biography and photograph of the author are not available.